Different impacts of two kinds of Pacific Ocean warming on tropical cyclone frequency over the western North Pacific

Guanghua Chen[1] and Chi-Yung Tam[2]

Received 9 November 2009; revised 6 December 2009; accepted 16 December 2009; published 14 January 2010.

[1] The present study examines the relationship of ENSO Modoki and canonical ENSO, respectively, with the tropical cyclone (TC) frequency over the western North Pacific (WNP) for the period 1960–2008. The TC frequency is significantly positively correlated with ENSO Modoki index. The Niño-3 index has a markedly negative (positive) correlation with the TC frequency in the northern (southeastern) portion of the WNP. In response to heating source related to El Niño Modoki, a large-scale cyclonic anomaly forms over the WNP. In contrast, during the canonical El Niño years, zonally-elongated heating source and sink exhibit a meridional dipole pattern, which induces an anticyclonic anomaly in the subtropics and a cyclonic anomaly near the equatorial central Pacific. Numerical experiments under the realistic mean state and heating profiles validate that the anomalous circulation responses to heating play essential roles in different modulations of two kinds of Pacific Ocean warming on the TC frequency. **Citation:** Chen, G., and C.-Y. Tam (2010), Different impacts of two kinds of Pacific Ocean warming on tropical cyclone frequency over the western North Pacific, *Geophys. Res. Lett.*, *37*, L01803, doi:10.1029/2009GL041708.

1. Introduction

[2] The El Niño and Southern Oscillation (ENSO), given its influence on the tropical climate, has significant impact on tropical cyclone (TC) activity in various ocean basins. Previous studies have examined the relationship between ENSO and the TC activity over the western North Pacific (WNP) [e.g., *Chan*, 2000; *Chia and Ropelewski*, 2002; *Wang and Chan*, 2002; *Wu et al*., 2004; *Chen et al*., 2006]. It was found that during El Niño years, there is a significant increase in the TC activity in the southeastern quadrant of WNP and a decrease in its northwestern quadrant; this situation is reversed during La Niña years.

[3] Recently, *Ashok et al*. [2007] have identified episodes of warming in the central Pacific Ocean, referred to as El Niño Modoki. In contrast to the canonical El Niño [e.g., *Rasmusson and Carpenter*, 1982], which occurs generally in the cold tongue region of the East Pacific Ocean, El Niño Modoki is characterized by warm sea surface temperature anomaly (SSTA) in the central tropical Pacific flanked by below-normal SSTA on its eastern and western sides. The two types of ENSO can lead to distinct climatic and synoptic variability in the global region. For example, El Niño Modoki is accompanied by two anomalous Walker circulation cells over the tropical Pacific, which is very different from the typical Walker cell perturbation during conventional ENSO events. Teleconnection patterns associated with El Niño Modoki also differ remarkably from those related to the canonical El Niño, giving rise to different geographical distributions of dry/wet conditions along the Pacific rim [*Weng et al*., 2007]. Distinct from the impacts of the canonical ENSO and the Indian Ocean Dipole (IOD) events, ENSO Modoki events can significantly influence the storm track activity in the mid latitudes of the Southern Hemisphere and thus reduce the storm-associated rainfall over southeastern Australia during austral winter [*Ashok et al*., 2009; *Cai and Cowan*, 2009].

[4] *Kim et al*. [2009] have found significant differences between the impacts of the two types of ENSO on TCs in the North Atlantic. However, hitherto there is no study distinguishing the impact of ENSO Modoki on the WNP TC activity from that of conventional ENSO. In fact, many previous studies adopt the Niño-3.4 SST index for identifying ENSO episodes [*Chan*, 2000; *Saunders et al*., 2000; *Chia and Ropelewski*, 2002]. Because of the geographical location of the Niño-3.4 region (170°W–120°W, 5°S–5°N), the use of this index possibly pick up SSTA signals associated with both conventional ENSO and ENSO Modoki, thus mixing up impacts related to the two different types of ENSO. For example, in the summer of 2004 when El Niño Modoki occurred [*Ashok et al*., 2007], a record-breaking number of ten typhoons made landfall in Japan [*Kim et al*., 2005]. However, during the same summer, Niño-3.4 SSTA remained positive, and, based on that, one should expect normal number of typhoons reaching the Japanese Archipelago according to previous studies. This highlights the need to separate the climatic impacts of these two phenomena.

[5] In addition, an increased frequency of El Niño Modoki events has been observed during the past few decades [*Ashok et al*., 2007], and the ratio of occurrence of El Niño Modoki events to canonical El Niño events is projected to increase as much as five times under global warming [*Yeh et al*., 2009]. Therefore, by using different indices to distinguish the two types of ENSO events, this study examines the different impacts of canonical ENSO and ENSO Modoki events on the TC frequency over the WNP, and proposes physical mechanisms responsible for their influences.

2. Data and Methodology

[6] The TC dataset over the WNP, which spans the period of 1960 to 2008, was obtained from the Joint Typhoon Warning Center (JTWC). Since about 85% of the total

[1]Center for Monsoon System Research, Institute of Atmospheric Physics, Chinese Academy of Sciences, Beijing, China.
[2]Guy Carpenter Asia-Pacific Climate Impact Centre, School of Energy and Environment, City University of Hong Kong, Hong Kong, China.

0094-8276/10/2009GL041708$05.00

annual number of TCs is observed from June to October (JJASO), the present study focuses on this extended period as well as the summer (JJA) and fall (SO) seasons to further explore its seasonal variation. Moreover, only TCs with maximum surface wind greater than $17ms^{-1}$ were considered. To examine the geographic distribution of TC formation, the tropical WNP (120°E–180, 0°–30°N) is partitioned into four domains. 150°E and 15°N serve as the borders between the east and west, the south and north, respectively. The northwestern, southwestern, southeastern and northeastern quadrants of the tropical WNP are designated as D_{NW}, D_{SW}, D_{SE}, and D_{NE}, respectively.

[7] The monthly sea surface temperature from the Hadley Center with a 1° × 1° horizontal resolution, the National Centers for Environmental Prediction (NCEP)–National Center for Atmospheric Research (NCAR) upper-air reanalysis with a 2.5° × 2.5° horizontal resolution from the same 1960–2008 period were used as observations. The monthly outgoing long wave radiation (OLR) data from the National Oceanic and Atmospheric Administration (NOAA) satellites on a 2.5° latitude–longitude grid from 1980–2008, which serve as a proxy for deep tropical convection [*Liebmann and Smith*, 1996], were also used in this study.

[8] The canonical ENSO can be defined by Niño-3 SST index which is a SSTA averaged over (150°W–90°W, 5°S–5°N). The ENSO Modoki phenomenon is quantified by ENSO Modoki index (EMI) constructed by *Ashok et al.* [2007], which can capture SST features in the central Pacific. EMI is computed based on the expression EMI = $[SSTA]_C - 0.5*[SSTA]_E - 0.5*[SSTA]_W$, where $[SSTA]_C$, $[SSTA]_E$ and $[SSTA]_W$ represent the SSTA averaged over the regions of (165°E–140°W, 10°S–10°N), (110°W–70°W, 15°S–5°N), and (125°E–145°E, 10°S–20°N), respectively. After removing the linear trends of the indices, the JJASO seasons during which the Niño-3 index and EMI are larger than one standard deviation are identified as the El Niño Modoki (1966, 1967, 1977, 1990, 1991, 1994, 2002, and 2004) and canonical El Niño events (1963, 1965, 1969, 1972, 1976, 1982, 1983, 1987, and 1997), respectively.

3. Relationships Between Two Kinds of Pacific Ocean Warming and TC Frequency

[9] In order to isolate the impact of ENSO Modoki and canonical ENSO on TC activity, the partial correlations of TC frequency over the whole WNP as well as each domain with the EMI and Niño-3 index during JJASO, JJA and SO seasons are calculated and listed in Table 1. According to Table 1, there is a significant correlation between EMI and TC frequency during the period of JJASO. This close relationship is mainly attributed to the correlation during summer (JJA). The correlation is weak during fall (SO). In contrast, Niño-3 index is almost uncorrelated with total TC frequency over the WNP basin. Similarly, an insignificant correlation is also obtained when Niño-3.4 index is used.

[10] Table 1 also shows very different geographic distribution of the correlation between the two types of ENSO events. In D_{NW} region, the correlation between the TC frequency and EMI is positive but weak, while the TC frequency is highly negatively correlated with Niño-3 index during summer and fall. In the southeastern part of the WNP (D_{SE}), two indices both show significant positive correlations with TC frequency, though the correlation coefficients related to EMI are less than those related to Niño-3 index. In addition, it is noted that, in the northeastern part of the WNP (D_{NE}), a significant negative correlation is detected for Niño-3 index, but the correlation is positive and insignificant for EMI. It is the reason why an insignificant relationship between the Niño-3.4 index and TC frequency in this region was found in previous studies. The above characteristics suggest the distinct impacts of the two types of ENSO events on the TC frequency.

[11] Since the correlations between TC frequency and these two indices are more significant during summer (Table 1), the circulation anomalies in JJA are examined in order to understand the impacts of the two types of ENSO events. Figures 1a and 1b show composites of meteorological fields for El Niño Modoki and canonical El Niño events. Although anomalously warm SST is present in the central Pacific during both El Niño Modoki and canonical El Niño events, the SST warming related to the former extends more meridionally and has a weaker zonal and meridional gradients of SST compared to its counterpart during canonical El Niño. The composites of OLR anomalies for the El Niño Modoki and canonical El Niño years from 1980 onwards are also given in Figure 1. For clarity, OLR anomalies are smoothed by applying a T15 truncation in order to remove smaller-scale features and to highlight the broad-scale convection pattern. Enhanced convection related to El Niño Modoki dominates a large fraction of tropical WNP spanning from the South China Sea to east of the dateline, while suppressed convection is found over the central-to-western maritime continent, as well as over eastern China, Korea and Japan. In contrast, the anomalous convection related to canonical El Niño is found to the east of 150°E with the center at 170°W. The convection just to its north is suppressed, which might be associated with sinking motion induced by strong positive heating over the equatorial Pacific. It is noteworthy that the strong anomalous OLR is zonally elongated and forms a meridional dipole pattern over the tropical WNP, which is distinct from the counterpart related to El Niño Modoki. In response to anomalous heating associated with different types of ENSO, the 850-hPa wind anomalies also exhibit markedly different patterns. During

Table 1. Partial Correlation Between TC Frequency and EMI and the Niño-3 Index Over the Whole WNP Basin As Well As Over Each of the Four Sub-Domains During the Periods of JJASO, JJA, and SO

	EMI					Niño-3				
	WNP	D_{NW}	D_{SW}	D_{SE}	D_{NE}	WNP	D_{NW}	D_{SW}	D_{SE}	D_{NE}
JJASO	0.31[a]	0.05	−0.16	0.39[b]	0.16	−0.13	−0.46[b]	0.06	0.56[b]	−0.41[b]
JJA	0.36[b]	0.07	0.04	0.35[a]	0.17	0.01	−0.38[b]	0.16	0.62[b]	−0.39[b]
SO	0.07	0.01	−0.29[a]	0.35[a]	0.09	−0.27	−0.33[a]	−0.29[a]	0.39[b]	−0.28

[a]Values exceeding the 95% confidence levels for a sample size of 49.
[b]Values exceeding the 99% confidence levels for a sample size of 49.

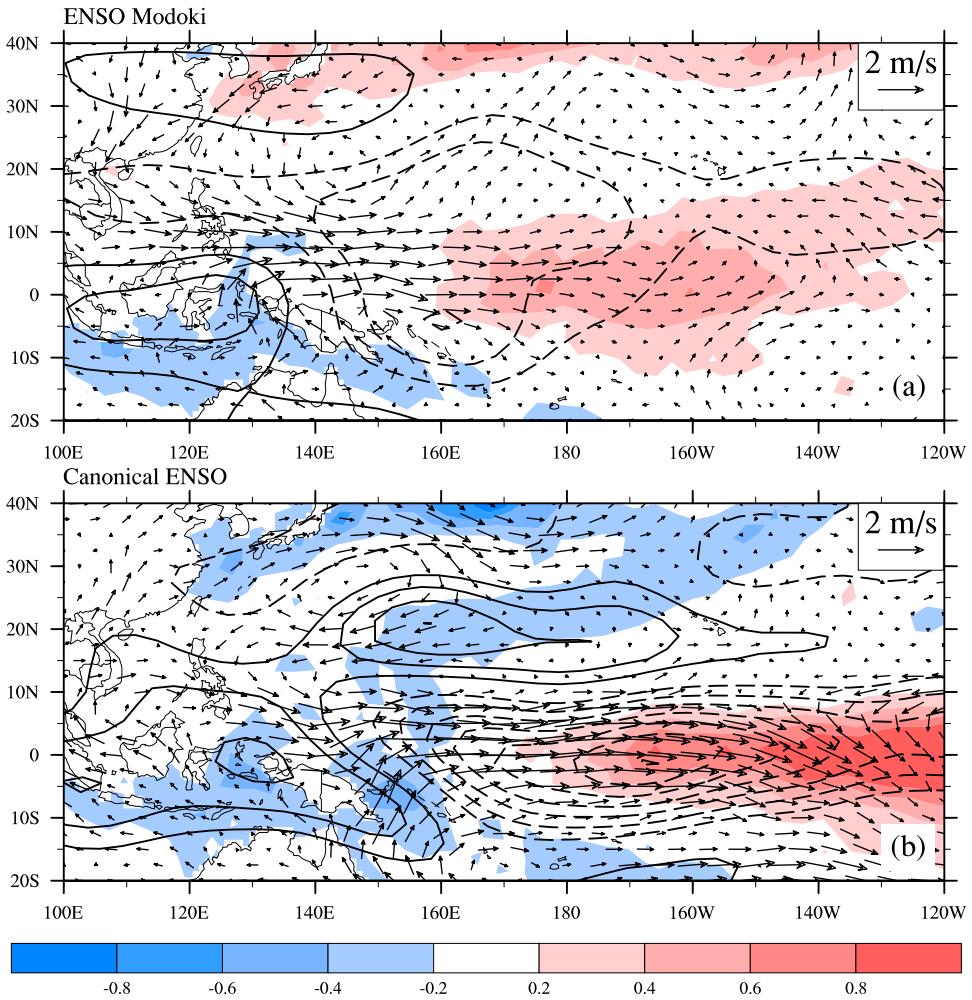

Figure 1. Composites of SSTA (shading; units: °C), 850-hPa wind anomalies (vectors, see scale arrow at the upper right; units of scale arrow: m s^{-1}) and OLR anomalies (dash/solid contours indicating negative/positive values; contour interval 3 W m^{-2}; zero contours omitted) during JJA for (a) El Niño Modoki and (b) canonical El Niño events. OLR anomalies are computed based on data starting from 1980 and with a T15 truncation applied for clarity.

the El Niño Modoki years, low-level westerly anomalies dominate the tropical WNP attaining their maximum near 140°E and meridionally extend to 15°N, which results in a large-scale anomalous cyclone to the southeast of Japan. Comparatively, during the canonical El Niño years, enhanced westerly anomalies at 850hPa are confined to the equatorial region south of 10°N, and moreover, their maximum shifts eastward beyond the dateline. This pattern is favorable for TC formation in the southeastern portion of WNP. On the other hand, accompanying the zonally elongated suppressed convection, the anomalous anticyclone prevails to the south of Japan during the canonical El Niño years, which is very different from the El Niño Modoki case. The anticyclonic flow anomaly is less conductive to TC genesis, leading to a significant negative correlation between TC frequency in the north portion of the WNP and Niño-3 index.

4. Results From a Simple Baroclinic Model

[12] To further delineate the relationship between circulation anomalies and heating for the two types of ENSO events, two numerical experiments using a simple baroclinic model are conducted to examine the atmosphere responses to different heating sources in the presence of the same realistic mean state. The model is constructed based on the dynamic core of the Geophysical Fluid Dynamics Laboratory AGCM [*Held and Suarez*, 1994; *Wang et al*., 2003]. It has equally distributed five sigma levels and a horizontal resolution of T42 is adopted.

[13] The model is linearized about a realistic three-dimensional summer mean (JJA) basic state, but otherwise retains full nonlinearity in the second order perturbation terms of the prediction equations. The basic state is taken from the long-time mean of the NCEP-NCAR reanalysis by linearly interpolating from the original standard pressure level data to the model sigma levels. Assuming a consistency between the distribution of the heating and OLR anomalies, the horizontal heating profiles are prescribed based on the OLR anomalies. To remove the effect of heating outside of the region of interest on large-scale circulation over the WNP and extract major features of the forcing, the anomalous OLR field is set to zero outside of the region (110°E–130°W, 10°S–30°N), and then truncated to T15 resolution in the same way as described in Section 3. Finally, the above-processed OLR anomalies are normalized by dividing by −9 W m^{-2} which is the minimum OLR

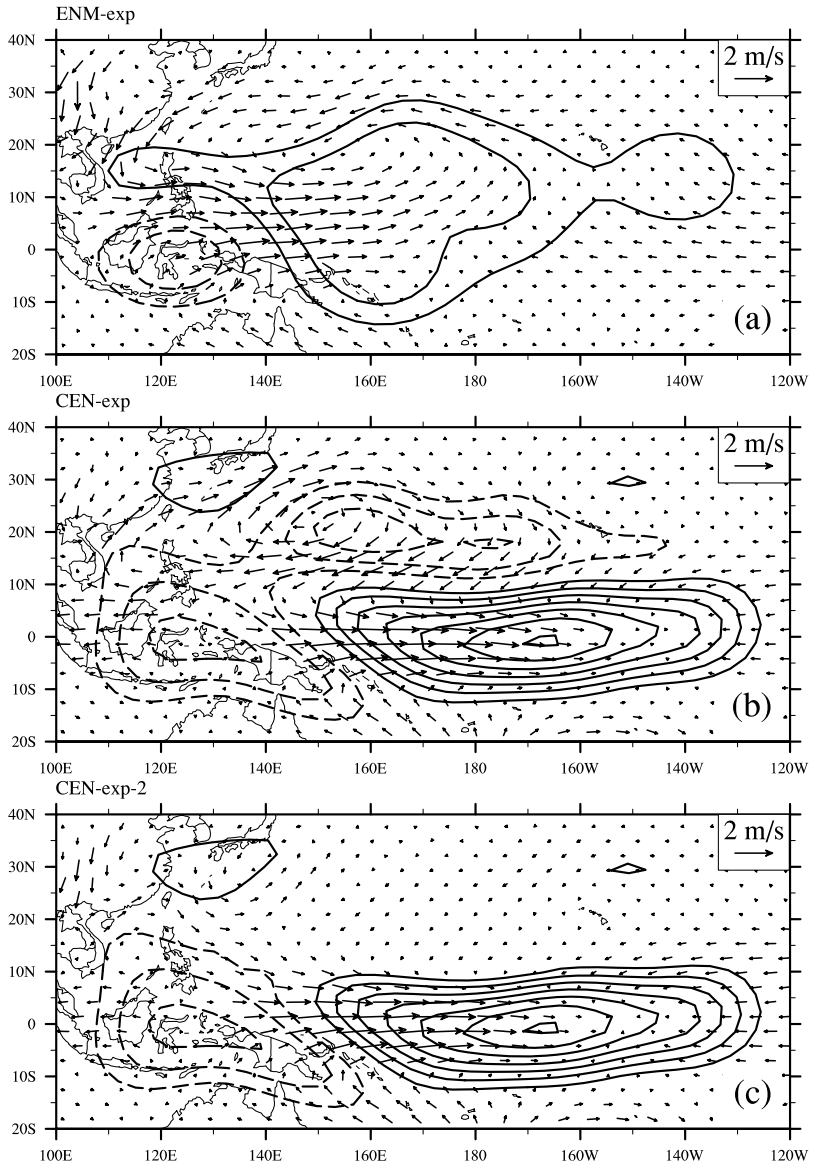

Figure 2. Simulated wind response (vectors, see scale arrows at top right; units: m s^{-1}) at 850 hPa in a simple baroclinic model to prescribed heating anomaly profiles (dash/solid contours representing negative/positive values of heating distribution at $\sigma = 0.5$; contour interval 0.2 K day^{-1}; zero contours omitted) for (a) El Niño Modoki and (b) canonical El Niño experiments. (c) Same as Figure 2b except with the WNP negative heating anomaly in the region (135°E–140°W, 10°–30°N) removed.

value during El Niño Modoki, and multiplied by 0.6 K day^{-1} to obtain the heating profiles for two numerical experiments corresponding to El Niño Modoki and cannocial El Niño events. The maximum heating is set at the level $\sigma = 0.5$. The amplitudes are reduced by a factor of 2 at $\sigma = 0.3$ and $\sigma = 0.7$ and by a factor of 5 at $\sigma = 0.1$ and $\sigma = 0.9$. This heating profile is approximately equivalent to 1.0 mm of precipitation per day basically in agreement with the observed anomalous precipitation [e.g., *Jin and Hoskins*, 1995; *Annamalai and Sperber*, 2005, *Ashok et al*., 2007].

[14] The integration results at day 30 are shown as the steady responses to prescribed heating sources. Figures 2a and 2b depict the prescribed heating profiles imposed at $\sigma = 0.5$ and the 850-hPa anomalous winds induced by heat sources for the El Niño Modoki experiment (ENM-exp) and the canonical El Niño experiment (CEN-exp). The heating profiles are almost consistent with those of OLR anomalies with slight differences near the domain boundaries.

[15] It can be seen that the simulated 850-hPa wind responses are in good agreement with the observed (Figure 1). In the ENM-exp (Figure 2a), a large-scale cyclonic circulation anomaly induced by zonally and meridionally extended heating dominates a large fraction of WNP. In other words, such a heating pattern leads to low-level positive vorticity anomalies over a large domain. This explains why there is an enhancement of TC occurrence in most domains of the WNP during El Niño Modoki years and therefore a significant correlation between TC frequency and EMI over the whole WNP (Table 1). On the other hand, in the CEN-exp, the positive heating near the equator is stronger and is shifted eastward, while a negative heating anomaly centered at about 20°N exists over WNP. Consistent with

such a cooling perturbation, an anticyclonic response in the low level is found north of 10°N over the WNP. The northeasterly wind related to this anticyclone penetrates into the deep Tropics and merges with the equatorial westerlies, forming a cyclonic shear pattern over near-equatorial WNP. Therefore, it is a meridional dipole of low-level circulation anomaly (cyclonic anomaly in the southeast part, anticyclonic anomaly in the northern part) over WNP that accounts for the significant negative correlation in the northern portion and significant positive correlation in the southeastern portion of the WNP between TC frequency and the Niño-3 index. Moreover, due to the mutual cancellation between enhanced and reduced TC frequency in the different domains, there is a weak relationship between total TC frequency over the whole WNP basin and canonical ENSO.

[16] In order to substantiate the importance of the heating sink to the north of the equatorial heating source in the development of anticyclonic circulation anomaly during the canonical El Niño years, a sensitive experiment (CEN-exp-2) is conducted, in which the negative heating anomaly in the region (135°E–140°W, 10°–30°N) is removed. The simulated results (Figure 2c) show that the original 850-hPa anticyclonic circulation anomaly vanishes, and even the cyclonic shear near the equator is weakened due to the disappearance of the northeasterlies related to the anticyclonic circulation anomaly. This suggests that the negative heating anomaly located in the subtropics during the canonical El Niño years plays a decisive role in inducing and maintaining the anticyclonic anomaly over the northern part of the WNP.

5. Concluding Remarks

[17] Using the NCEP reanalysis variables and TC dataset for the period 1960–2008, the present study examines the different impacts of ENSO Modoki and canonical ENSO events on TC frequency over WNP during boreal summer and fall. Different from the Niño-3.4 index which may mix up eastern Pacific warming and central Pacific warming, EMI and Niño-3 index can distinguish two types of Pacific warming events. The results show that TC frequency in the WNP basin is significantly positively correlated with EMI during JJA. On the contrary, the relationship of TC frequency and Niño-3 index becomes weakened owing to mutual cancellation between enhanced and reduced TC frequency in the different domains. Less TCs occur in the northern part of WNP, while more TCs form in the southeastern part of WNP during the canonical El Niño years. These differences can be attributed to the different large-scale circulation anomalies between the two types of ENSO events. An anomalous cyclonic circulation in response to a broad heating source dominates over the WNP during the El Niño Modoki years. In contrast, in response to the a zonally elongated and meridional dipole pattern of heating over the WNP during the canonical El Niño years (heating source being located in the equatorial central Pacific and heating sink just north of it), an anomalous anticyclonic circulation persists in the subtropics, while an cyclonic shear associated with the equatorial westerly anomalies is dominant in the southeast part of the WNP.

[18] A baroclinic numerical model is used to validate the relationship between wind anomalies and heating forcing. A realistic summer (JJA) mean state serves as the basic state. The heating source/sink, whose profiles are similar to those of the observed OLR anomalies, is prescribed to force the atmosphere in the presence of the same realistic mean state. The simulated results are qualitatively consistent with the observed, suggesting that the different distributions of heating related to two types of ENSO events can play essential roles in the distinct modulations on the TC frequency over the WNP basin. In the end, it is worthwhile noting that, with a probable increasing tendency of El Niño Modoki occurrence in terms of observed data and scenario simulation under climate change projections, the present results urge that the modulation of ENSO Modoki on TC activity should be taken into account in TC activity prediction in the context of global warming.

[19] **Acknowledgments.** We would like to thank Renguang Wu of COLA for helpful modification for our manuscript and Karumuri Ashok for discussions and encouragement. This study is supported by the National Natural Science Foundation of China (grant 40921160379), the Special Scientific Research Project for Public Interest (grant GYHY200806009) and City University of Hong Kong (grant 9360126).

References

Annamalai, H., and K. R. Sperber (2005), Regional heat sources and the active and break phases of boreal summer, *J. Atmos. Sci.*, *62*, 2726–2748, doi:10.1175/JAS3504.1.

Ashok, K., S. K. Behera, S. A. Rao, H. Weng, and T. Yamagata (2007), El Niño Modoki and its possible teleconnection, *J. Geophys. Res.*, *112*, C11007, doi:10.1029/2006JC003798.

Ashok, K., C. Y. Tam, and W. J. Lee (2009), ENSO Modoki impact on the Southern Hemisphere storm track activity during extended austral winter, *Geophys. Res. Lett.*, *36*, L12705, doi:10.1029/2009GL038847.

Cai, W., and T. Cowan (2009), La Niña Modoki impacts Australia autumn rainfall variability, *Geophys. Res. Lett.*, *36*, L12805, doi:10.1029/2009GL037885.

Chan, J. C. L. (2000), Tropical cyclone activity over the western North Pacific associated with El Niño and La Niña events, *J. Clim.*, *13*, 2960–2972, doi:10.1175/1520-0442(2000)013<2960:TCAOTW>2.0.CO;2.

Chen, T. C., S. Y. Wang, and M. C. Yen (2006), Interannual variation of the tropical cyclone activity over the western North Pacific, *J. Clim.*, *19*, 5709–5720, doi:10.1175/JCLI3934.1.

Chia, H. H., and C. F. Ropelewski (2002), The interannual variability in the genesis location of tropical cyclones in the northwest Pacific, *J. Clim.*, *15*, 2934–2944, doi:10.1175/1520-0442(2002)015<2934:TIVITG>2.0.CO;2.

Held, I. M., and M. J. Suarez (1994), A proposal for the intercomparison of the dynamical cores of atmospheric general circulation models, *Bull. Am. Meteorol. Soc.*, *75*, 1825–1830, doi:10.1175/1520-0477(1994)075<1825:APFTIO>2.0.CO;2.

Jin, F. F., and B. J. Hoskins (1995), The direct response to tropical heating in a baroclinic atmosphere, *J. Atmos. Sci.*, *52*, 307–319, doi:10.1175/1520-0469(1995)052<0307:TDRTTH>2.0.CO;2.

Kim, H. M., P. J. Webster, and J. A. Curry (2009), Impact of shifting patterns of Pacific Ocean warming on North Atlantic tropical cyclones, *Science*, *325*, 77–80, doi:10.1126/science.1174062.

Kim, J. H., C. H. Ho, and C. H. Sui (2005), Circulation features associated with the record-breaking typhoon landfall on Japan in 2004, *Geophys. Res. Lett.*, *32*, L14713, doi:10.1029/2005GL022494.

Liebmann, B., and C. A. Smith (1996), Description of a complete (interpolated) OLR dataset, *Bull. Am. Meteorol. Soc.*, *77*, 1275–1277.

Rasmusson, E. M., and T. H. Carpenter (1982), Variations in tropical sea surface temperature and surface wind fields associated with the Southern Oscillation/El Niño, *Mon. Weather Rev.*, *110*, 354–384, doi:10.1175/1520-0493(1982)110<0354:VITSST>2.0.CO;2.

Saunders, M. A., R. E. Chandler, C. J. Merchant, and F. P. Roberts (2000), Atlantic hurricanes and NW Pacific typhoons: ENSO spatial impacts on occurrence and landfall, *Geophys. Res. Lett.*, *27*, 1147–1150, doi:10.1029/1999GL010948.

Wang, B., and J. C. L. Chan (2002), How strong ENSO events affect tropical storm activity over the western North Pacific, *J. Clim.*, *15*, 1643–1658, doi:10.1175/1520-0442(2002)015<1643:HSEEAT>2.0.CO;2.

Wang, B., R. G. Wu, and T. Li (2003), Atmosphere-warm ocean interaction and its impacts on Asian-Australian Monsoon variation, *J. Clim.*, *16*, 1195–1211, doi:10.1175/1520-0442(2003)16<1195:AOIAII>2.0.CO;2.

Weng, H., K. Ashok, S. Behera, S. A. Rao, and T. Yamagata (2007), Impacts of recent El Niño Modoki on dry/wet conditions in the Pacific rim during boreal summer, *Clim. Dyn.*, *29*, 113–129, doi:10.1007/s00382-007-0234-0.

Wu, M. C., W. L. Chang, and W. M. Leung (2004), Impacts of El Niño–Southern Oscillation events on tropical cyclone landfalling activity in the western North Pacific, *J. Clim.*, *17*, 1419–1428, doi:10.1175/1520-0442(2004)017<1419:IOENOE>2.0.CO;2.

Yeh, S. W., J. S. Kug, B. Dewitte, M. H. Kwon, B. P. Kirtman, and F. F. Jin (2009), El Niño in a changing climate, *Nature*, *461*, 511–514, doi:10.1038/nature08316.

G. Chen, Center for Monsoon System Research, Institute of Atmospheric Physics, Chinese Academy of Sciences, P.O. Box 2718, Beijing 100190, China. (cgh@mail.iap.ac.cn)

C.-Y. Tam, Guy Carpenter Asia-Pacific Climate Impact Centre, School of Energy and Environment, City University of Hong Kong, Hong Kong, China.